Progress In Electromagnetics Research, Vol. 149, 205–216, 2014

Metasurface Synthesis for Time-Harmonic Waves: Exact Spectral and Spatial Methods

Mohamed A. Salem*, Karim Achouri, and Christophe Caloz

(*Invited Paper*)

Abstract—Two exact approaches to synthesize metasurfaces for time-harmonic waves are discussed. The first approach is a spectral approach based on wave momentum conservation. Here, the spectral approach is applied to scalar and paraxial wave transformations. This approach effectively allows the arbitrary translation of the transformation plane parallel to the metasurface. The second approach is a direct-space approach based on the extraction of the susceptibility tensors of the metasurface elements. This approach is applied to vectorial field transformation and can be used for single or multiple transformations. An example of wave transformation by a metasurface is illustrated for each of the two approaches.

1. INTRODUCTION

Metasurfaces are promising devices for electromagnetic field control beyond conventional means. As two-dimensional metamaterial structures, they do not suffer from the disadvantages associated with volumetric metamaterials, such as bulkiness, excessive losses and fabrication difficulty [1]. Metasurfaces have been employed to control the reflection and transmission of electromagnetic waves [2], realize generalized refraction [3] and reflection-less refraction [4] for plane-waves, single-layer perfect absorbers [6] and reciprocal [7] and non-reciprocal [8, 9] polarization rotators.

The metasurface synthesis problem is stated as follows; a metasurface is an infinitesimally thin planar sheet with an arbitrary lateral extension. The sheet is composed of scattering elements much smaller than the operating wavelength. Given a monochromatic time-harmonic electromagnetic field incident on the metasurface and given a specific scattered field, it is required to determine the description of the metasurface scattering elements to produce the transformation between the incident and the scattered fields. An illustration of the synthesis problem configuration is shown in Figure 1. In what follows, we assume a harmonic-time dependence $\exp(-i\omega t)$ and that the metasurface is directed along the z-direction and located at $z = 0$.

So far, only two approaches have been introduced to formally accomplish this transformation, the first is based on momentum transformation [10], and the second is based on susceptibility tensor extraction [11]. In this paper, we discuss these two exact approaches to synthesize the metasurface given the incident and the scattered fields. The first approach is spectral and yields a metasurface description in the momentum space of the waves [10]. This approach is best suited for scalar and paraxial waves for its simplicity and its capability of arbitrarily translating the plane of the scattered field parallel to the metasurface. The second approach is spatial and yields a metasurface description in terms of susceptibilities [11]. This approach is best suited for vectorial field transformation due to its direct

Received 5 October 2014, Accepted 29 October 2014, Scheduled 4 November 2014

Invited paper for the Commemorative Collection on the 150-Year Anniversary of Maxwell's Equations.

* Corresponding author: Mohamed A. Salem (mohamed.salem@polymtl.ca).

The authors are with the Department of Electrical Engineering, École Polytechnique de Montréal, Montréal, Québec H2T 1J3, Canada.

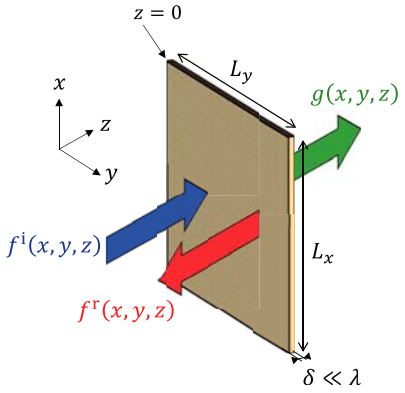

Figure 1. An illustration of an electromagnetic transformation by a metasurface. The metasurface is a non-uniform structure of extent $L_x \times L_y$ with sub-wavelength thickness ($\delta \ll \lambda$) and located at $z = 0$. It is required to find the electromagnetic description of the metasurface to transform a specified incident wave $f^{\mathrm{i}}(x, y, 0^-)$ into a specified reflected wave $f^{\mathrm{r}}(x, y, 0^-)$ and an arbitrary specified transmitted wave $g(x, y, 0^+)$.

connection with the metasurface scattering elements. We note that the synthesis approaches discussed here are the first step in metasurface design. Complete metasurface design further requires determining the exact shapes of the scattering elements, which is out of the scope of this paper. However, the scattering elements may be directly determined using lookup maps [3], iterative analysis [4], or dipole response approximation [5].

This paper is organized as follows; first the spectral synthesis method based on momentum transformation for scalar and paraxial fields is introduced Section 2. The section starts with the derivation of the momentum transformation relations followed by the reverse propagator operator. An example of a metasurface that transforms an incident Gaussian beam into a hypergeometric-Gaussian vortex beam is shown for illustration. Next, the spatial synthesis method based on scattering element susceptibilities for vectorial fields is introduced in Section 3. The section starts with the derivation of the element susceptibilities from the metasurface boundary conditions followed by the application of the method for metasurface synthesis for electromagnetic wave transformation. An example of a metasurface that acts as a perfect lens for an electric dipole is shown for illustration. The conclusion of the work is given in Section 4. Two appendices are included; the first presents the derivation of the momentum transformation relation for the spectral approach and the second presents Maxwell's equations in the sense of distributions for a planar sheet.

2. SPECTRAL SYNTHESIS METHOD: MOMENTUM TRANSFORMATION

The electromagnetic wave momentum (wavevector) is conserved in homogeneous media. Subsequently, a forced change in any of the momentum components necessarily changes the other components such that the total momentum is conserved. Hence, by forcing local changes onto the transverse components of the wavevector, the wavevector may be locally varied such that the wavefront is reshaped in a controlled fashion. The interaction between the metasurface and the fields is local in space, i.e., the difference between the field at a certain point on one side of the metasurface and the same point on the opposite side is solely determined by the metasurface transfer function at the same point. Formal mathematical derivation is given in appendix A. The local interaction in the direct space translates into a convolution relation in the momentum space. Although momentum space manipulation is convolutional in nature, it allows for superior light manipulation at distance compared to direct space manipulation, as will be shown. The momentum transformation method thus emerges as best suited candidate for metasurface synthesis since it can effectively manipulate the transverse components of the wavevector.

The following sub-section establishes the scalar approach for momentum transformation, which deals with scalar fields, such as acoustic fields and paraxially approximate fields encountered in optics.

2.1. The Scalar Transform

In the scalar case, for a thin metasurface, the interaction between the fields and the metasurface is local, i.e., linear-shift variant. For a metasurface located at $z = 0$ in the Cartesian coordinate system with the fields $f(x, y)$ at $z = 0^-$ and $g(x, y)$ at $z = 0^+$, this linear-shift variant relation reads

$$\begin{aligned} g(x,y) &= \iint_S f\left(x',y'\right) h\left(x',y';x,y\right) dx'dy', \\ &= \iint_S f\left(x',y'\right) \delta\left(x'-x,y'-y\right) \eta(x,y)\, dx'dy', \\ &= f(x,y)\,\eta(x,y), \end{aligned} \tag{1}$$

where the z-coordinate is suppressed, S denotes the plane of the metasurface and $h(x', y'; x, y)$ is the generalized transfer function of the metasurface, which reduces to $\eta(x, y)$ due to local interaction.

The fundamental transformation between the direct space and the momentum space in the vicinity of the metasurface plane is established through the two-dimensional Fourier transform pair,

$$\begin{aligned} \tilde{f}(k_x,k_y;0) &= \frac{1}{2\pi}\iint_{-\infty}^{\infty} f(x,y;0)\, e^{-i[k_x x+k_y y]} dxdy, \\ f(x,y;0) &= \frac{1}{2\pi}\iint_{-\infty}^{\infty} \tilde{f}(k_x,k_y;0)\, e^{i[k_x x+k_y y]} dk_x dk_y, \end{aligned} \tag{2}$$

where the tilde denotes momentum space quantities, and (k_x, k_y) are the transverse components of the wave momentum, $\mathbf{k}$. In the momentum space, relation (1) is expressed as a convolutional relation reading $\tilde{g} = \tilde{f} * \tilde{\eta}$. Alternatively, this relation is rewritten to express the metasurface function explicitly as

$$\tilde{\eta}(k_x,k_y) = \tilde{g}(k_x,k_y) * \tilde{\zeta}(k_x,k_y) \tag{3}$$

with $\zeta = 1/f$.

2.2. Plane Translation of Scattered Field

Equation (3) by itself does not offer much advantage over its direct space counterpart (1). However, it could be argued that the momentum space representation offers better insight into the required metasurface dynamic range of momentum variation, i.e., the lower and upper bounds of momentum variation that need to be induced by the metasurface in order to achieve the required transformation. This assists in synthesizing the metasurface using scattering elements. On the other hand, the superior advantage of the momentum space representation is clearly apparent when wave manipulation at a distance is required. For instance, to specify the transmitted field at a distance $z = d$ away from the metasurface plane, it is sufficient to introduce a momentum space operator to propagate the momentum components of $\tilde{g}$ from $z = d$ back to the metasurface plane at $z = 0$. This operator, named the reverse propagator, is a Fourier propagator taking the simple form

$$\tilde{\Phi}(k_x,k_y;d) = \exp\left(-i\sqrt{k^2-k_x^2-k_y^2}\,d\right). \tag{4}$$

Extending (4) with (3) yields the complete momentum transformation equation

$$\tilde{\eta}(k_x,k_y) = \left[\tilde{g}(k_x,k_y)\,\tilde{\Phi}(k_x,k_y;d)\right] * \tilde{\zeta}(k_x,k_y). \tag{5}$$

We note here that the function $\eta(x, y)$ may be reduced to the commonly used optical transfer function (OTF) [12], which takes the form

$$\tilde{g}(k_x,k_y) = \tilde{f}^{\mathrm{i}}(k_x,k_y)\,\tilde{\eta}_{\mathrm{OTF}}(k_x,k_y),$$

where $\tilde{\eta}_{\mathrm{OTF}}$ is the OTF and superscript i denotes the incident wave. This reduction takes places under certain special conditions, such as normal incidence, large electrical size of the surface and when reflection is ignored. Under these conditions, the momentum space convolution reduces to a simple product and

η reduces to the OTF, e.g., in the case of normal incidence without reflection, $\tilde{f}(k_x, k_y) = \delta(k_x)\delta(k_y)$ reducing the convolution to a product.

We also note that if a passive metasurface design is required, additional conditions must be invoked, namely, that the intensity of the incident wave is equal to or greater than the combined intensities of the reflected and transmitted waves at every point on the metasurface, viz. $|f^{\mathrm{i}}(x, y, 0^-)|^2 \geq |f^{\mathrm{r}}(x, y, 0^-)|^2 + |g(x, y, 0^+)|^2$, with the superscript r denoting the reflected wave.

The momentum transformation technique is not limited to scalar wave manipulation and could be extended to vectorial fields as well as demonstrated in [10]. It should be noted though that the vector nature of the problem introduces an extra level of complication, where the metasurface becomes a vector mode transformer in the momentum space.

2.3. Illustrative Example: Vortex Hypergeometric-Gaussian Beam

Hypergeometric-Gaussian (HyG) beams are a class of paraxial wave solutions with a complex amplitude that is proportional to a confluent hypergeometric function. The beam intensity profile is characterized by a single bright ring with the field amplitude vanishing at its center. HyG beams carry topological charges, i.e., their phasefronts are helical, and thus have a singular phase profile. In quantum mechanics, HyG beams describe the eigenfunctions of the photon orbital angular momentum, and since they carry orbital angular momentum, they are of interest in applications, such as micro- and nano-particle manipulation and orbital angular momentum multiplexing [13].

The HyG beam field is defined as

$$g_{\mathrm{HyG}}(\rho, \phi, z) = \frac{\Gamma\left(1 + |m| + \frac{p}{2}\right)}{\Gamma(|m| + 1)} \frac{i^{|m|+1} \chi^{|m|/2} \xi^{p/2}}{[\xi + i]^{1+|m|/2+p/2}} e^{im\phi - i\chi} {}_1F_1\left(-\frac{p}{2}, |m| + 1; \frac{\chi}{\xi}\frac{[\xi + i]}{[\xi - i]}\right), \tag{6}$$

where $\Gamma(x)$ is the gamma function, ${}_1F_1(a, b; x)$ is the confluent hypergeometric function, w_0 is the beam waist, $p \geq -|m|$ is a real valued parameter, m is the topological charge, p and m together specify the HyG mode, $\chi = \rho^2/(w_0^2[\xi + i])$, and $\xi = z/z_{\mathrm{R}}$ with $z_{\mathrm{R}} = \pi w_0^2/\lambda$ the Rayleigh range.

HyG beams are unstable in the presence of small perturbations below the Rayleigh range, z_{R}, meaning that one mode can easily degenerate into others. Hence it is of interest to generate the HyG beam directly beyond the Rayleigh range in order to avoid the inherent beam instability. In this example, the HyG beam is generated by illuminating the metasurface by an ordinary Gaussian beam,

$$f_{\mathrm{GB}}(\rho, \phi, z) = \frac{w_0}{w(z)} \exp\left(-\frac{r^2}{w(z)^2} - ik\left[z + \frac{r^2}{2R(z)}\right] - i\vartheta(z)\right), \tag{7}$$

where $r^2 = \rho^2 + z^2$, $R(z) = z[1 + (z_{\mathrm{R}}/z)^2]$ is the beam radius of curvature, $w(z) = w_0[1 + (z/z_{\mathrm{R}})^2]^{1/2}$ the beam waist with w_0 the beam waist at $z = 0$, and $\vartheta(z) = \arctan(z/z_{\mathrm{R}})$ the Gouy phase. The k-space representation of the field expressions in (6) and (7) are substituted into (5), where the reverse propagator in this particular example is used as an advance propagator, i.e., it translates the beam profile in the negative z-direction as opposed to the conventional positive translation. The purpose of the propagator here is to generate the HyG beam at the plane of the metasurface with the characteristics of a HyG at $z = z_{\mathrm{R}}$, thus avoiding the instability region of the beam. The propagator is given by

$$\tilde{\Phi} = \exp\left(i\sqrt{k^2 - k_x^2 - k_y^2}\, z_{\mathrm{R}}\right).$$

Figure 2 shows the synthesized metasurface function required to convert an ordinary Gaussian beam into a vortex hypergeometric-Gaussian beam. Figures 2(a) and 2(b) respectively depict the phases of the incident ordinary Gaussian beams and the transmitted hypergeometric-Gaussian beam. The incident beam has a beam waist $w_0 = \lambda$ and zero Guoy phase and is transformed into a vortex hypergeometric-Gaussian beam with the same beam waist, a topological charge $m = 4$, and $p = 10$. The transmitted hypergeometric-Gaussian beam is advance-propagated to distance $z = z_{\mathrm{R}}$ to avoid the beam instability range. The magnitude and phase of the metasurface function required to achieve the transformation are plotted in 2(c) and 2(d), respectively. It is interesting to note that even though the vorticities of the metasurface and the transmitted beam have the same topological charge magnitude, $|m| = 4$, they are in counter rotation. This difference in rotation is necessary for the conservation of the total orbital angular momentum, since the incident beam does not carry orbital angular momentum.

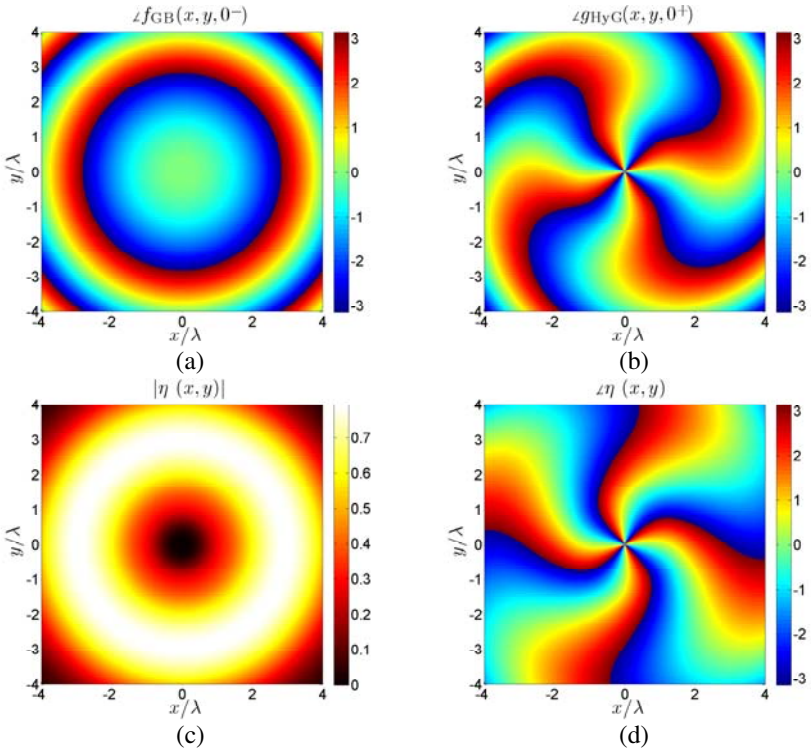

Figure 2. Transformation of an ordinary Gaussian beam into a hypergeometric-Gaussian beam carrying orbital angular momentum. The phase of the incident Gaussian beam is depicted in (a) with the effect of the phase-front curvature visible in the radial variation. The phase of the transmitted hypergeometric-Gaussian beam is depicted in (b) with four distinctive phase transitions corresponding to a vorticity with topological charge $m = 4$. The magnitude and phase of the spatial metasurface function to achieve the transformation are plotted in in (c) and (d), respectively.

3. DIRECT SYNTHESIS METHOD: SUSCEPTIBILITY TENSORS

Since a the presence of the metasurface induces a discontinuity in the electromagnetic field, a rigorous treatment of such discontinuity is necessary. One approach, proposed in [14], takes advantage of expressing the quantities in Maxwell's equations in the sense of distributions. This representation allows for a generalized set of boundary conditions to be devised. More details on the expression of Maxwell's equations in the sense of distributions are given in Appendix B. The concept of generalized boundary conditions has been worked out for the case of a source-free thin planar surface in [15], yielding the following generalized sheet transition conditions for a surface at $z = 0$

$$\hat{z} \times \Delta\mathbf{H} = -i\omega\mathbf{P}_\perp - \hat{z} \times \nabla_\perp M_z, \tag{8a}$$

$$\hat{z} \times \Delta\mathbf{E} = i\omega\mu\mathbf{M}_\perp - \hat{z} \times \nabla_\perp \left(\frac{P_z}{\epsilon}\right), \tag{8b}$$

$$\hat{z} \cdot \Delta\mathbf{D} = -\nabla \cdot \mathbf{P}_\perp, \tag{8c}$$

$$\hat{z} \cdot \Delta\mathbf{B} = -\mu\nabla \cdot \mathbf{M}_\perp, \tag{8d}$$

where $\mathbf{E}$, $\mathbf{H}$, $\mathbf{D}$ and $\mathbf{B}$ are respectively the electric, magnetic, displacement and magnetic flux fields. The delta terms represent field differences on both sides of the surface, e.g., $\Delta\mathbf{E} = \mathbf{E}(x, y, 0^+) - \mathbf{E}(x, y, 0^-)$, and the subscript $\perp$ denotes the transverse vector components with respect to z. The quantities ϵ and μ are respectively the permittivity and permeability, and $\mathbf{P}$ and $\mathbf{M}$ are respectively the electric and magnetic surface polarization densities. The polarization densities are generally expressed in terms of

the acting (local) field as

$$\mathbf{P} = \epsilon N \langle \overline{\overline{\alpha}}_{\mathrm{ee}} \rangle \mathbf{E}_{\mathrm{act}} + \epsilon N \langle \overline{\overline{\alpha}}_{\mathrm{em}} \rangle \sqrt{\frac{\mu}{\epsilon}} \mathbf{H}_{\mathrm{act}}, \tag{9a}$$

$$\mathbf{M} = N \langle \overline{\overline{\alpha}}_{\mathrm{me}} \rangle \sqrt{\frac{\epsilon}{\mu}} \mathbf{E}_{\mathrm{act}} + N \langle \overline{\overline{\alpha}}_{\mathrm{mm}} \rangle \mathbf{H}_{\mathrm{act}}, \tag{9b}$$

where $\langle \overline{\overline{\alpha}}_{\mathrm{ab}} \rangle$ are the averaged polarizabilities around a given scattering element; the subscripts e and m respectively stand for electric and magnetic; N is the number of scattering elements per unit area. The acting (local) field is the average field on both sides of the surface taking into account the contribution due to the coupling between the scattering elements, but does not include the field produced by the elements. To account for the acting field due to sub-wavelength scattering elements, each scattering element is modeled by a small disk encompassing electric and magnetic current dipoles. In [15], the fields of these disks are expressed in terms of $\mathbf{P}$ and $\mathbf{M}$, which permits eliminating the acting field expressions from (9). Additionally, the effective surface susceptibilities could be used in place of the polarizabilities for a complete macroscopic description of the surface. Hence,

$$\mathbf{P} = \epsilon \overline{\overline{\chi}}_{\mathrm{ee}} \overline{\mathbf{E}} + \epsilon \overline{\overline{\chi}}_{\mathrm{em}} \sqrt{\frac{\mu}{\epsilon}} \overline{\mathbf{H}}, \tag{10a}$$

$$\mathbf{M} = \overline{\overline{\chi}}_{\mathrm{me}} \sqrt{\frac{\epsilon}{\mu}} \overline{\mathbf{E}} + \overline{\overline{\chi}}_{\mathrm{mm}} \overline{\mathbf{H}}, \tag{10b}$$

where the field terms on the right-hand side are the average on both sides of the surface, e.g., $\overline{\mathbf{E}} = [\mathbf{E}(x, y, 0^+) + \mathbf{E}(x, y, 0^-)]/2$. Note that assuming propagation in the positive z-direction, the field at $z = 0^-$ could be expressed as $\mathbf{E}(x, y, 0^-) = \mathbf{E}^{\mathrm{i}}(x, y, 0^-) + \mathbf{E}^{\mathrm{r}}(x, y, 0^-)$, where the superscripts i and r respectively stand for incident and reflected. Similarly, the field at $z = 0^+$ could be expressed as the transmitted field $\mathbf{E}(x, y, 0^+) = \mathbf{E}^{\mathrm{t}}(x, y, 0^+)$.

3.1. Extraction of Surface Susceptibilities

From the previous analysis, the synthesis method could be formulated as an inverse problem where the electromagnetic fields are defined everywhere and the properties of the metasurface are unknown. This method, as detailed in [11], is thus based on solving equations (8) for the components of the susceptibility tensors with relations (10). Equations (8a) and (8b) involve the derivatives of the normal components of the polarization densities and yield a set of coupled inhomogeneous partial differential equations. In this scenario, solutions of the inverse problem is typically not available in analytic form and may be found by means of numerical analysis. Nevertheless, under the assumption that the metasurface is infinitesimally thin and hence no physical scattering elements could be employed to induce a variation in P_z, it is acceptable to enforce $P_z = 0$. Additionally, the condition $M_z = 0$ is enforced to further simplify the analysis without severely limiting the transformation capabilities of the metasurface. These conditions admit obtaining closed-form solutions for the susceptibilities. In what follows, only equations (8a) and (8b) will be used as they combine all the transverse components of the fields which are sufficient to completely describe the electromagnetic fields on each side of the metasurface according to the uniqueness theorem. These two vectorial equations represent a set a four scalar equations relating the transverse electric and magnetic fields to the effective surface susceptibilities. Therefore, the inverse problem is determined for a given arrangement of four effective susceptibilities.

3.2. Synthesis for Single Transformation

By inserting (10) into (8a) and (8b), and dropping out the equations with the normal field components, the following relations are obtained

$$\begin{pmatrix} \Delta H_y \\ -\Delta H_x \end{pmatrix} = i\omega\epsilon \begin{pmatrix} \chi_{\mathrm{ee}}^{xx} & \chi_{\mathrm{ee}}^{xy} \\ \chi_{\mathrm{ee}}^{yx} & \chi_{\mathrm{ee}}^{yy} \end{pmatrix} \begin{pmatrix} \overline{E}_x \\ \overline{E}_y \end{pmatrix} + i\omega\epsilon \sqrt{\frac{\mu}{\epsilon}} \begin{pmatrix} \chi_{\mathrm{em}}^{xx} & \chi_{\mathrm{em}}^{xy} \\ \chi_{\mathrm{em}}^{yx} & \chi_{\mathrm{em}}^{yy} \end{pmatrix} \begin{pmatrix} \overline{H}_x \\ \overline{H}_y \end{pmatrix}, \tag{11a}$$

$$\begin{pmatrix} -\Delta E_y \\ \Delta E_x \end{pmatrix} = i\omega\mu \sqrt{\frac{\epsilon}{\mu}} \begin{pmatrix} \chi_{\mathrm{me}}^{xx} & \chi_{\mathrm{me}}^{xy} \\ \chi_{\mathrm{me}}^{yx} & \chi_{\mathrm{me}}^{yy} \end{pmatrix} \begin{pmatrix} \overline{E}_x \\ \overline{E}_y \end{pmatrix} + i\omega\mu \begin{pmatrix} \chi_{\mathrm{mm}}^{xx} & \chi_{\mathrm{mm}}^{xy} \\ \chi_{\mathrm{mm}}^{yx} & \chi_{\mathrm{mm}}^{yy} \end{pmatrix} \begin{pmatrix} \overline{H}_x \\ \overline{H}_y \end{pmatrix}. \tag{11b}$$

The linear system (11) consists of four equations with sixteen unknowns. This system is underdetermined and requires further processing to become solvable. Two approaches may be considered for the processing, the first approach enforces certain relations between the susceptibilities, and the second eliminates twelve of the unknown susceptibilities. In what follows, the two approaches are investigated. For the first approach, certain physical conditions between the susceptibility components are readily available, such as the conditions for reciprocity and for losslessness. According to [16, 17], the conditions for reciprocity are given as

$$\overline{\overline{\chi}}_{\mathrm{ee}}^{\mathrm{T}} = \overline{\overline{\chi}}_{\mathrm{ee}}, \quad \overline{\overline{\chi}}_{\mathrm{mm}}^{\mathrm{T}} = \overline{\overline{\chi}}_{\mathrm{mm}}, \quad \overline{\overline{\chi}}_{\mathrm{me}}^{\mathrm{T}} = -\overline{\overline{\chi}}_{\mathrm{em}}, \tag{12}$$

where superscript T denotes the transpose, and the conditions for losslessness are given as

$$\overline{\overline{\chi}}_{\mathrm{ee}}^{\mathrm{T}} = \overline{\overline{\chi}}_{\mathrm{ee}}^{*}, \quad \overline{\overline{\chi}}_{\mathrm{mm}}^{\mathrm{T}} = \overline{\overline{\chi}}_{\mathrm{mm}}^{*}, \quad \overline{\overline{\chi}}_{\mathrm{me}}^{\mathrm{T}} = \overline{\overline{\chi}}_{\mathrm{em}}^{*}, \tag{13}$$

where superscript $*$ denotes the complex conjugate.

It should be noted that enforcing such relations between susceptibilities limits the types of possible electromagnetic transformations achievable with the metasurface. On the other hand, employing the second approach, where only four susceptibility components exist, provides a general synthesis method for arbitrary electromagnetic transformations. Since the linear system consists of four equations, then one of the four possible susceptibilities is chosen per equation. This yields a total number of 256 possible arrangements. Depending on the required transformation and the application, many of these arrangements may violate the reciprocity or the losslessness conditions and may be eliminated.

For simplicity and without loss of generality, the following analysis assumes a reciprocal metasurface where only the diagonal terms of the susceptibility tensors are retained. Solving (11) under this assumption yields

$$\chi_{\mathrm{ee}}^{xx} = \frac{\Delta H_y}{i\omega\epsilon\overline{E}_x}, \tag{14a}$$

$$\chi_{\mathrm{ee}}^{yy} = \frac{-\Delta H_x}{i\omega\epsilon\overline{E}_y}, \tag{14b}$$

$$\chi_{\mathrm{mm}}^{xx} = \frac{-\Delta E_y}{i\omega\mu\overline{H}_x}, \tag{14c}$$

$$\chi_{\mathrm{mm}}^{yy} = \frac{\Delta E_x}{i\omega\mu\overline{H}_y}. \tag{14d}$$

To demonstrate the relationship linking the transmitted field to the incident field and the susceptibilities, a reflectionless metasurface is assumed to simplify the analysis. Hence solving (14) for the transmitted field yields

$$E_x^{\mathrm{t}} = -E_x^{\mathrm{i}} + \frac{8E_x^{\mathrm{i}} + i4\chi_{\mathrm{mm}}^{yy}\mu\omega H_y^{\mathrm{i}}}{4 + \chi_{\mathrm{ee}}^{xx}\chi_{\mathrm{mm}}^{yy}\epsilon\mu\omega^2}, \tag{15a}$$

$$E_y^{\mathrm{t}} = -E_y^{\mathrm{i}} + \frac{8E_y^{\mathrm{i}} - i4\chi_{\mathrm{mm}}^{xx}\mu\omega H_x^{\mathrm{i}}}{4 + \chi_{\mathrm{mm}}^{xx}\chi_{\mathrm{ee}}^{yy}\epsilon\mu\omega^2}, \tag{15b}$$

$$H_x^{\mathrm{t}} = -H_x^{\mathrm{i}} + \frac{8H_x^{\mathrm{i}} - i4\chi_{\mathrm{ee}}^{yy}\epsilon\omega E_y^{\mathrm{i}}}{4 + \chi_{\mathrm{mm}}^{xx}\chi_{\mathrm{ee}}^{yy}\epsilon\mu\omega^2}, \tag{15c}$$

$$H_y^{\mathrm{t}} = -H_y^{\mathrm{i}} + \frac{8H_y^{\mathrm{i}} + i4\chi_{\mathrm{ee}}^{xx}\epsilon\omega E_x^{\mathrm{i}}}{4 + \chi_{\mathrm{ee}}^{xx}\chi_{\mathrm{mm}}^{yy}\epsilon\mu\omega^2}. \tag{15d}$$

Equations (15) show that the transmitted field components depend on their own counterparts and their orthogonal dual, e.g., E_x^{t} depends on E_x^{i} and H_y^{i}. This is an important synthesis condition that has to be accounted for in the metasurface design process.

3.3. Illustrative Example: Holographic Repeater

A holographic repeater is a device that constructs an image of a primary source at a desired distance away from that source. There is significant interest in such repeaters, particularly in point-to-point free-space communication applications. Previous research work in this area employed near-field patterned plates [18] or antenna arrays and a metascreen [19] to replicate the source image. In this example, a holographic repeater is constructed employing a metasurface illuminated by an ideal dipole. The metasurface is located midway between the dipole source and its holographic image.

The main difficulty in successfully reconstructing the source image is that away from the source, the evanescent components of the field decay in magnitude in contrast to the propagating components which only incur a phase change. A perfect source reconstruction based on superlenses made out of doubly-negative metamaterials was proposed in [20]. Here, an equivalent two-dimensional perfect lens is constructed by choosing the appropriate susceptibilities for the metasurface. Moreover, if the metasurface has an infinite extension, then the evanescent field components can be successfully transmitted and a perfect construction of the holographic image of the source at a distance is possible. Nevertheless, the constructed holographic image of the source can only radiate in the forward direction (away from the metasurface), in contrast to the actual dipole source. Any causal radiation from the holographic image in the backward direction would necessarily require the presence of a source located farther away from the metasurface and the holographic image.

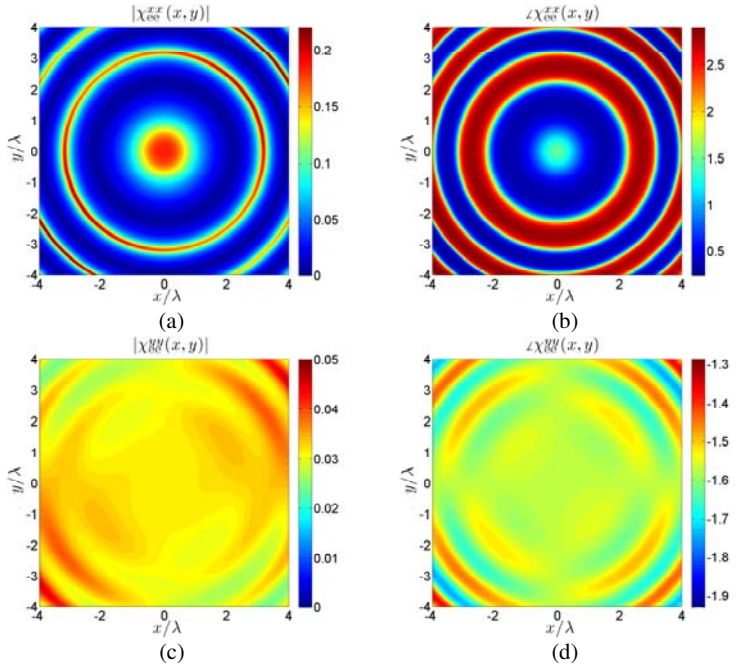

Figure 3. The electric susceptibilities of a reciprocal holographic reaper metasurface. The metasurface is illuminated by the field radiated from an $\hat{x}$-oriented electric dipole located at $z = -10\lambda$. The constructed holographic image appears at $z = 10\lambda$ and is completely causal (i.e., no backward radiation). The magnitude and phase of χ_{ee}^{xx} are plotted in (a) and (b), respectively. The corresponding values of χ_{ee}^{yy} are plotted in (c) and (d), respectively.

In this example, the dipole source is oriented along $\hat{x}$ and is located at $x = 0, y = 0$ and $z = -10\lambda$. It is required to construct a holographic image of the dipole at $x = 0, y = 0$ and $z = 10\lambda$. The non-zero incident field components are thus given by

$$E_x^{\text{i}}(r_0, \theta_0, \phi) = \frac{ie^{ikr}}{8\pi r^3 \epsilon\omega}\left[1 + k^2r^2 - ikr + \left(-3 + k^2r^2 - 3ikr\right)\cos(2\theta)\right]\cos^2(\phi) + \frac{ie^{ikr}}{4\pi r^3 \epsilon\omega}\left[-1 + k^2r^2 + ikr\right]\sin^2(\phi),$$

$$E_y^{\mathrm{i}}(r_0,\theta_0,\phi) = \frac{e^{ikr}}{8\pi r^3\epsilon\omega}\left[3i - ik^2r^2 + 3kr\right]\sin^2(\theta)\sin(2\phi),$$

$$E_z^{\mathrm{i}}(r_0,\theta_0,\phi) = \frac{e^{ikr}}{8\pi r^3\epsilon\omega}\left[3i - ik^2r^2 + 3kr\right]\sin(2\theta)\cos(\phi),$$

$$H_y^{\mathrm{i}}(r_0,\theta_0,\phi) = \frac{e^{ikr}}{4\pi r^2}\left[-1 + ikr\right]\cos(\theta),$$

$$H_z^{\mathrm{i}}(r_0,\theta_0,\phi) = \frac{e^{ikr}}{4\pi r^2}\left[1 - ikr\right]\sin(\theta)\sin(\phi),$$

where $r_0^2 = x^2 + y^2 + (z+10\lambda)^2$ and $\theta_0 = \arccos([z+10\lambda]/r_0)$. The transmitted field at $z = 0^+$ is the phase conjugate of the incident field at $z = 0^-$, and the metasurface in this example acts as a phase conjugating surface in transmission mode. The field difference and average are thus respectively proportional to the imaginary and real parts of the incident field, e.g., $\Delta\mathbf{E} = 2\mathrm{Im}\{\mathbf{E}^{\mathrm{i}}\}$ and $\overline{\mathbf{E}} = \mathrm{Re}\{\mathbf{E}^{\mathrm{i}}\}$. The susceptibilities are found in a straightforward fashion under the assumption of reciprocity using (14).

Figure 3 depicts the electric susceptibility of the synthesized metasurface. The magnitude and phase of χ_{ee}^{xx} are plotted in 3(a) and 3(b), respectively, while the corresponding values of χ_{ee}^{yy} are plotted in 3(c) and 3(d), respectively. The magnetic susceptibilities near the center of the metasurface are similar to their electric orthogonal duals.

4. CONCLUSION

In this paper, the two exact approaches to synthesize a metasurface capable of electromagnetic transformation have been described. The first approach is spectral in the wave momentum space and yields a spectral description of the metasurface function. This approach is most suitable for scalar and paraxial waves for its simplicity and the physical insight it provides. The momentum approach is extensible to vectorial fields as well, but the extensions entails more involved analysis, which may subtract from the ease of application. Here, only the scalar transformation based on momentum is shown to demonstrate the concept. The second approach is a direct space approach based on extracting the surface electric and magnetic susceptibilities. This approach is more suitable for vectorial field transformation.

In the momentum transformation case, a relation between the spectral components on each side of the metasurface is established. The metasurface transfer function is introduced to induce changes in the transverse components of the wave on one side of the metasurface to those of the wave on the other side of the metasurface while conserving the total wave momentum. This spectral representation has the added advantage when manipulating the wave at a distance far away from the metasurface is required. An illustrative example is shown, where an incident ordinary Gauss beam is transformed into a vortex hypergeometric-Gaussian beam beyond its instability region.

On the other hand, in the direct space transformation case, the differences and the averages of the fields on both sides of the metasurface are linked to the electric and magnetic susceptibilities. These relations yield an underdetermined system of coupled nonlinear equations. The system of equations can be linearized by assuming no transformation of the field components normal to the surface. The resulting linear system could then be made determined either by enforcing certain relations between the susceptibility components, such as reciprocity and losslessness, or by selectively choosing to retain only a specific set of susceptibility components, which extends the transformation possibilities of the metasurface.

The presented systematic approaches to synthesize a metasurface are the two possible exact approaches to achieve electromagnetic transformation. Nevertheless, these approaches are the first step in the overall metasurface design process. Once the metasurface description, whether as a spectral function or in terms of the electric and magnetic susceptibilities, is determined, the following step is to map this description to physical scattering elements. This mapping could be carried out using iterative full-wave analysis for example. Nevertheless, the presented approaches may be considered as useful interpretations of Maxwell's equations for metasurface applications.

APPENDIX A. METASURFACE-FIELD LOCAL INTERACTION IN SPACE AND MOMENTUM CONSERVATION

A formal representation of (3) is derived applying the distribution theory for the momentum discontinuity in the metasurface plane. First, the difference between the fields at the two sides of the metasurface is considered

$$\begin{aligned} g\left(x,y\right)-f\left(x,y\right)&=\Lambda\left(x,y\right),\\ \tilde{g}\left(k_x,k_y\right)-\tilde{f}\left(k_x,k_y\right)&=\tilde{\Lambda}\left(k_x,k_y\right), \end{aligned} \tag{A1}$$

where $\Lambda(x,y)$ is the field difference. Equation (A1) seems a priori contradictory, since $\tilde{\Lambda}(k_x,k_y)$ has to be zero due to the momentum conservation. However, this apparent contradiction vanishes when the momenta are considered in the sense of distributions, i.e., generalized functions describing the physics. This may be shown by using the Fourier transform property of distributions [21]

$$\langle\mathcal{F}^{-1}\left\{\tilde{\Lambda}\right\},\tilde{\varphi}\rangle=\langle\tilde{\Lambda},\mathcal{F}^{-1}\left\{\tilde{\varphi}\right\}\rangle, \tag{A2}$$

where $\mathcal{F}^{-1}\{\tilde{\psi}\}$ is the inverse Fourier transform of $\tilde{\psi}$, $\tilde{\varphi}$ is a well-behaved, i.e., smooth and has a compact support, testing function. This well-behavior of $\tilde{\varphi}$ is also necessary when describing causal physical phenomena. Hence,

$$\langle\psi(x,y),\varphi(x,y)\rangle=\iint_{-\infty}^{\infty}\psi(x,y)\varphi(x,y)dxdy.$$

Choosing the testing function to be the general transfer function of the metasurface, and considering the momentum conservation relation, (A2) reduces to

$$\langle\mathcal{F}^{-1}\left\{\tilde{\Lambda}\right\},\tilde{h}\rangle=\langle0,\mathcal{F}^{-1}\left\{\tilde{h}\right\}\rangle,$$

which requires $\mathrm{supp}[\tilde{\Lambda}]=0$, i.e., $\tilde{\Lambda}=\tilde{\alpha}(k_x,k_y)\delta(k_x,k_y)$, with $\tilde{\alpha}$ an arbitrary spectral function. Inserting this relation into (2) and changing the order of the integrals, assuming the well-behavior of h, recovers (1) by choosing $\alpha(x,y)=[\eta(x,y)-1]f(x,y)$.

APPENDIX B. MAXWELL EQUATIONS IN THE SENSE OF DISTRIBUTIONS FOR A PLANAR SHEET

If a function $f(z)$ is discontinuous at $z=0$, it can be rewritten as

$$f(z)=f_+(z)U(z)+f_-(z)U(-z), \tag{B1}$$

where $U(x)$ is the Heaviside unit step function and $f_\pm(z)$ denote the extension of the function for $z>0$ and $z<0$, respectively. Since Maxwell's equations imply spatial and temporal derivatives, it is required to understand the behavior of $df(z)/dz$ across the discontinuity. By properties of the distributions, we have

$$\left\langle U',\phi\right\rangle=-\left\langle U,\phi'\right\rangle=\left\langle\delta,\phi\right\rangle, \tag{B2}$$

the derivative of the Heaviside unit step function is the Dirac delta. Thus the derivative of (B1) with respect to z can be expressed as

$$\frac{\mathrm{d}}{\mathrm{d}z}f(z)=\left\{f'_+(z)U(z)+f'_-(z)U(-z)\right\}+(f_+(0)-f_-(0))\delta(z)=\left\{f'\right\}+[[f]]\,\delta(z), \tag{B3}$$

where the term $\{\cdot\}$ is the regular part defined for $z\neq0$, and the term $[[\cdot]]$ is the singular part defined at the discontinuity. Equation (B1) can thus be expressed as

$$f(z)=\{f(z)\}+\sum_{j=0}^{M}f_j\delta^{(j)}(z), \tag{B4}$$

where M is an integer, f_j a constant coefficient, and $\delta^{(j)}(z)$ the j-th derivative of the Dirac delta. This representation is essential for the proper formulation of the boundary conditions across the discontinuity. To illustrate the process, this formulation is applied to the Maxwell-Ampère equation,

$$\nabla \times \mathbf{H} = \mathbf{J} - i\omega\mathbf{D}, \tag{B5}$$

with the fields $\mathbf{H}, \mathbf{D}$ and the electric current $\mathbf{J}$ taking the form of (B4). Equation (B5) then reads

$$\nabla \times \mathbf{H} = \nabla_\perp \times \{\mathbf{H}\} + \hat{z} \times \frac{\partial}{\partial z}\{\mathbf{H}\} + \sum_{j=0}^{M} \nabla_\perp \times \mathbf{H}_j \delta^{(j)}(z) + \sum_{j=0}^{M} \hat{z} \times \frac{\partial}{\partial z}\mathbf{H}_j \delta^{(j)}(z), \tag{B6}$$

where the relation $\nabla = \nabla_\perp + \hat{z}\frac{\partial}{\partial z}$ is employed. The second term on the right-hand side of (B6) can be written in form of (B3), whereas the last term on the right-hand side of the same equation solemnly includes derivatives of the Dirac delta function since $\mathbf{H}_j$ is not a function of z. Therefore, equation (B6) becomes

$$\nabla \times \mathbf{H} = \nabla_\perp \times \{\mathbf{H}\} + \hat{z} \times \left\{\frac{\partial}{\partial z}\mathbf{H}\right\} + \hat{z} \times [[\mathbf{H}]]\,\delta(z) \sum_{j=0}^{M} \nabla_\perp \times \mathbf{H}_j \delta^{(j)}(z) + \sum_{j=0}^{M} \hat{z} \times \mathbf{H}_j \delta^{(j+1)}(z), \tag{B7}$$

where the first two terms on the right-hand side of (B7) are the regular parts. Equating the derivative order of the Dirac delta functions, we have, for $j = 0$

$$\hat{z} \times [[\mathbf{H}]] + \nabla_\perp \times \mathbf{H}_0 = \mathbf{J}_0 - i\omega\mathbf{D}_0, \tag{B8}$$

and for $j \geq 1$

$$\hat{z} \times \mathbf{H}_{j-1} + \nabla_\perp \times \mathbf{H}_j = \mathbf{J}_j - i\omega\mathbf{D}_j. \tag{B9}$$

Similarly, the same process is applied to the rest of Maxwell's equations; for $j = 0$

$$\hat{z} \times [[\mathbf{E}]] + \nabla_\perp \times \mathbf{E}_0 = -\mathbf{K}_0 + i\omega\mathbf{B}_0, \tag{B10a}$$

$$\hat{z} \cdot [[\mathbf{D}]] + \nabla_\perp \times \mathbf{D}_0 = \rho_0, \tag{B10b}$$

$$\hat{z} \cdot [[\mathbf{B}]] + \nabla_\mathrm{t} \times \mathbf{B}_0 = m_0, \tag{B10c}$$

and for $j \geq 1$

$$\hat{z} \times \mathbf{E}_{j-1} + \nabla_\perp \times \mathbf{E}_j = -\mathbf{K}_j + i\omega\mathbf{B}_j, \tag{B11a}$$

$$\hat{z} \cdot \mathbf{D}_{j-1} + \nabla_\perp \times \mathbf{D}_j = \rho_j, \tag{B11b}$$

$$\hat{z} \cdot \mathbf{B}_{j-1} + \nabla_\perp \times \mathbf{B}_j = m_j, \tag{B11c}$$

where $\mathbf{K}$ is the magnetic current, and ρ and m are respectively the electric and magnetic charges.

The relations for $j = 0$ are the thus the constituents of the boundary conditions for time-harmonic waves, whereas the relations for $j \geq 1$ are compatibility relations that can be used recursively to find the unknown terms in (B8) and (B10). In the case of a thin sheet that induces field discontinuities, the higher order source quantities vanish. Moreover, by assuming that the distributions have a finite support, i.e., M is finite, then all the terms with index $j > M$ identically vanish. Recursively applying the finite support approximation yields that all terms with index $j > 0$ also identically vanish. Hence, relations (B9) and (B11) can be modified into

$$\hat{z} \times \mathbf{H}_0 = 0, \tag{B12a}$$

$$\hat{z} \times \mathbf{E}_0 = 0, \tag{B12b}$$

$$\hat{z} \cdot \mathbf{D}_0 = 0, \tag{B12c}$$

$$\hat{z} \cdot \mathbf{B}_0 = 0. \tag{B12d}$$

By making use of $\mathbf{D} = \epsilon\mathbf{E} + \mathbf{P}$ and $\mathbf{B} = \mu\mathbf{H} + \mu\mathbf{M}$, and inserting (B12) into (B8) and (B10), the final expression for a source-free single planar sheet boundary conditions are

$$\hat{z} \times [[\mathbf{H}]] = -i\omega\mathbf{P}_{0,\perp} + \nabla_\perp \times \mathbf{M}_{0,\parallel}, \tag{B13a}$$

$$\hat{z} \times [[\mathbf{E}]] = i\omega\mu\mathbf{M}_{0,\perp} + \nabla_\perp \times \frac{1}{\epsilon}\mathbf{P}_{0,\parallel}, \tag{B13b}$$

$$\hat{z} \cdot [[\mathbf{D}]] = -\nabla_\perp \cdot \mathbf{P}_{0,\perp}, \tag{B13c}$$

$$\hat{z} \cdot [[\mathbf{B}]] = -\mu\nabla_\perp \cdot \mathbf{M}_{0,\perp}, \tag{B13d}$$

where the subscript $\parallel$ denotes the normal component.

REFERENCES

1. Holloway, C. L., E. F. Kuester, J. A. Gordon, J. O'Hara, J. Booth, and D. R. Smith, "An overview of the theory and applications of metasurfaces: the two-dimensional equivalents of metamaterials," *IEEE Antennas Propag. Mag.*, Vol. 54, No. 2, 10–35, Apr. 2012.
2. Holloway, C. L., M. A. Mohamed, E. F. Kuester, and A. Dienstfrey, "Reflection and transmission properties of a metafilm: With an application to a controllable surface composed of resonant particles," *IEEE Trans. Electromagn. Compat.*, Vol. 47, No. 4, 853–865, Nov. 2005.
3. Yu, N., P. Genevet, M. A. Kats, F. Aieta, J.-P. Tetienne, F. Capasso, and Z. Gaburro, "Light propagation with phase discontinuities: generalized laws of reflection and refraction," *Science*, Vol. 334, No. 6054, 333–337, 2011.
4. Pfeiffer, C. and A. Grbic, "Metamaterial Huygens' surfaces: Tailoring wave fronts with reflectionless sheets," *Phys. Rev. Lett.*, Vol. 110, 197401, May 2013.
5. Niemi, T., A. O. Karilainen, and S. A. Tretyakov, "Synthesis of Polarization Transformers," *IEEE Trans. Antennas Propag.*, Vol. 61, No. 6, 3102–3111, Jun. 2013.
6. Ra'di, Y., V. S. Asadchy, and S. A. Tretyakov, "Total absorption of electromagnetic waves in ultimately thin layers," *IEEE Trans. Antennas Propag.*, Vol. 61, No. 9, 4606–4614, Sept. 2013.
7. Shi, H., A. Zhang, S. Zheng, J. Li, and Y. Jiang, "Dual-band polarization angle independent 90° polarization rotator using twisted electric-field-coupled resonators," *Appl. Phys. Lett.*, Vol. 104, No. 3, 2014.
8. Kodera, T., D. L. Sounas, and C. Caloz, "Artificial faraday rotation using a ring metamaterial structure without static magnetic field," *Appl. Phys. Lett.*, Vol. 99, No. 3, 2011.
9. Sounas, D. L., T. Kodera, and C. Caloz, "Electromagnetic modeling of a magnet-less non-reciprocal gyrotropic metasurface," *IEEE Trans. Antennas Propag.*, Vol. 61, No. 1, 221–231, Jan. 2013.
10. Salem, M. A. and C. Caloz, "Manipulating light at distance by a metasurface using momentum transformation," *Opt. Express*, Vol. 22, No. 12, 14 530–14 543, Jun. 2014.
11. Achouri, K., M. A. Salem, and C. Caloz, "General metasurface synthesis based on susceptibility tensors," arXiv:1408.0273, Aug. 2014.
12. Goodman, J. W., *Introduction to Fourier Optics*, 2nd Edition, McGraw-Hill, New York, NY, 1996.
13. Kotlyar, V. V. and A. A. Kovalev, "Family of hypergeometric laser beams," *J. Opt. Soc. Am. A*, Vol. 25, No. 1, 262–270, Jan. 2008.
14. Idemen, M. M., *Discontinuities in the Electromagnetic Field*, John Wiley & Sons, Hoboken, NJ, 2011.
15. Kuester, E. F., M. A. Mohamed, M. Piket-May, and C. L. Holloway, "Averaged transition conditions for electromagnetic fields at a metafilm," *IEEE Trans. Antennas Propag.*, Vol. 51, No. 10, 2641–2651, Oct. 2003.
16. Kong, J. A., *Electromagnetic Wave Theory*, John Wiley & Sons, New York, NY, 1986.
17. Lindell, I. V., A. H. Sihvola, S. A. Tretyakov, and A. J. Viitanen, *Electromagnetic Waves in Chiral and Bi-Isotropic Media*, Artech House, Boston, MA, 1994.
18. Grbic, A., L. Jiang, and R. Merlin, "Near-field plates: Subdiffraction focusing with patterned surfaces," *Science*, Vol. 320, No. 5875, 511–513, 2008.
19. Markley, L. and G. V. Eleftheriades, "Meta-screens and near-field antenna-arrays: A new perspective on subwavelength focusing and imaging," *Metamaterials*, Vol. 5, No. 2–3, 97–106, 2011.
20. Pendry, J. B., "Negative refraction makes a perfect lens," *Phys. Rev. Lett.*, Vol. 85, 3966–3969, Oct. 2000.
21. Strichartz, R. S., *A Guide to Distribution Theory and Fourier Transforms*, World Scientific, River Edge, NJ, 2003.